Unsteady Normal Force on an Airfoil in a Periodically Stalled Inlet Flow

FRANKLIN O. CARTA*
United Aircraft Research Laboratories, East Hartford, Conn.

The effect of a circumferential inlet velocity distortion on the normal force response and stall characteristics of a rotating blade in an axial-flow turbomachine was analytically investigated by considering the response of an airfoil subjected to a periodically varying incidence angle. A hypothetical distortion profile that produced both large and small rates of change of incidence was employed in the analysis; the number of distortions per revolution was varied, and a substantial penetration of the incidence angle into the stall region occurred at maximum distortion. Unsteady flow effects, including dynamic stall behavior, were introduced into the analysis by using an empirical set of unsteady aerodynamic data previously obtained on an NACA 0012 airfoil oscillating in pitch over a wide range of test conditions. Use was also made of the unsteady potential flow theory of Theodorsen. It was found that the severity of the dynamic stall was intimately related to the rate at which the incidence angle decreased from its maximum value; slowly decreasing incidence produced the severest dynamic stall, whereas rapidly decreasing incidence yielded very little dynamic stall.

Nomenclature†

a = dimensionless distance of pivot axis aft of the midchord, in semichords, Eq. (A1)
A = dimensionless angular velocity parameter, Eq. (1)
b = semichord, ft, Eq. (1)
B = dimensionless angular acceleration parameter, Eq. (2)
$C(k)$ = Theodorsen circulation function
C_N = normal force coefficient, Eq. (6)
$C_{N_{\alpha^s}}$ = slope of normal force coefficient curve, Eq. (A7)
E = number of excitations per revolution
f = oscillatory frequency in pitch, cps, Fig. 2
$F(k)$ = real part of Theodorsen function, Eq. (A2)
$G(k)$ = imaginary part of Theodorsen function, Eq. (A2)
k = $b\omega/V$ = reduced frequency parameter, Eq. (1)
k_e = equivalent reduced frequency parameter, Eq. (B1)
L_h, L_α = unsteady lift functions, Eq. (A1)
M = Mach number, Fig. 2
n = Fourier index
N = normal force, lb, Eq. (A1)
R = rotational speed, rpm, Eq. (3)
t = time, sec, Eq. (A1)
T = disturbance period, sec
U, W = unsteady aerodynamic functions in Eqs. (A5) and (A6)
V = resultant velocity, fps, Fig. 1
α = incidence angle, deg or rad, Eq. (1)
α_M = mean incidence angle, deg or rad, Eq. (1)
$\alpha_{\max}$, $\alpha_{\min}$ = maximum and minimum values of incidence angle, deg or rad
α_g = geometric incidence angle, deg
α_s = stalling angle, deg or rad
$\bar{\alpha}$ = amplitude of angular motion, deg or rad, Eq. (1)
λ = fraction of circumferential period, Eq. (5)
ρ = air density, slug/ft^3
σ = dimensionless stall angle parameter defined by Eq. (5)
ϕ = circumferential position, rad, Eq. (3)
ϕ_D = circumferential position, deg, Eq. (3)
ω = oscillatory frequency in pitch, rad/sec, Eq. (A1)
Ω = rotational speed, rad/sec
$(\dot{}), (\ddot{})$ = first and second time derivatives
$(\ )_I$ = imaginary part
$(\ )_n$ = quantity associated with the nth harmonic
$(\ )_R$ = real part

Presented as Paper 67-18 at the AIAA 5th Aerospace Sciences Meeting, New York, January 23–26, 1967; submitted January 3, 1967; revision received May 24, 1967. [4.01]

* Supervisor, Aeroelastics Group, Aerophysics Section. Member AIAA.

† Where applicable, the equation or figure in which the symbol is first introduced or used is noted in the definition.

Introduction

THE performance of an axial-flow compressor can be seriously compromised by the presence of a nonuniform circumferential velocity distribution in the inlet of the compressor. Such an inlet velocity distortion could be caused by a poorly designed engine inlet, flow separation from some portion of the inlet cowl arising from a locally large incidence angle, or even by scavenging of a thick boundary layer from some adjacent aerodynamic surface. Whatever the cause, the primary effect will generally be the same; viz., if there exists, circumferentially, some region of reduced axial velocity, a compressor blade travelling at a constant rotational speed will experience a periodic change in incidence angle, as shown in Fig. 1. The aerodynamic performance of a blade in a distorted flow will depart from some nominal operating condition; the degree of this departure will depend largely on such parameters as the number of distortions per revolution, the circumferential extent of each distortion, the magnitude of each distortion, and the rate at which incidence-angle changes due to the distortion take place.

In an effort to treat the essentials of the distortion problem, use was made of a large body of oscillating airfoil data (unpublished) obtained under corporate sponsorship. In these tests an isolated NACA 0012 airfoil was oscillated in pitch about its quarter-chord over a wide range of incidence angle, amplitude of motion, frequency of oscillation, and Mach number. Of relevance to the present study is the fact that an increase in oscillatory frequency (with all other parameters held fixed) appears to reduce the effects of stalling. This is illustrated in Fig. 2, which shows that a low-frequency motion causes the normal force to drop sharply after reaching its peak value, whereas a high-frequency motion causes the normal force to remain at a moderately high level, commensurate with the instantaneous incidence angle, throughout the cycle of motion. Thus it appears that the rate of change of incidence angle has a major effect on the unsteady aerodynamic response of a lifting surface operating near or beyond the steady-state stall point.

As part of the original experimental study, a correlation of the results was made which permitted the use of these data to approximate the unsteady normal force resulting from a

nonsinusoidal motion. In principle, any aerodynamic system having a time variation in incidence angle can be approximately analyzed by the use of these data, with the accuracy of the representation largely dependent on the ability of the given distribution of incidence angle and its first two time derivatives to approximate the motion. Such an approximation is being used in this study. In addition to the restriction just cited, this approximation will also be limited in the present case by the inability of isolated airfoil data to predict accurately the response of a cascaded blade system.

Theory

Empirical Data

The unsteady normal force coefficient was determined for an isolated, two-dimensional NACA 0012 airfoil which had a 2-ft chord and which was oscillated sinusoidally in pitch about its quarter-chord. In this test program, the unsteady normal force coefficient C_N was measured over a wide range of parameter values. As shown in Fig. 2, this unsteady normal force coefficient for each test condition was plotted as a function of instantaneous incidence angle α to form a closed loop. The data obtained in this fashion were then crossplotted and correlated to yield a tabulation of the normal force coefficient as a function of incidence angle and its first two dimensionless time derivatives A and B. These quantities are defined in terms of the instantaneous angle of attack $\alpha = \alpha_M + \bar{\alpha}\sin\omega t$, by the equations

$$A = b\dot{\alpha}/V = \pm k[\bar{\alpha}^2 - (\alpha - \alpha_M)^2]^{1/2} \quad (1)$$

$$B = b^2\ddot{\alpha}/V^2 = -k^2(\alpha - \alpha_M) \quad (2)$$

Family of Distortion Profiles

Although in the original study the data were obtained for a sinusoidal motion of the test airfoil, the correlation procedure previously described provided a set of data which could be applied to a nonsinusoidal, periodic motion. The only requirements for an adequate representation were that the first and second derivatives of the motion be reasonably well behaved and that the values of these derivatives lie generally within the bounds of the available data. Application of these data to the present study depends on the same general requirements, and it should be clearly understood that the results obtained herein have merit primarily in the qualitative differences that are shown to exist between the various cases considered.

A fundamental characteristic of any distortion analysis concerns the shape of the distortion profile. Typically, this can be represented in terms of the incidence-angle variation as a function of circumferential position around the rotor. This is represented by the hypothetical curve in Fig. 3,

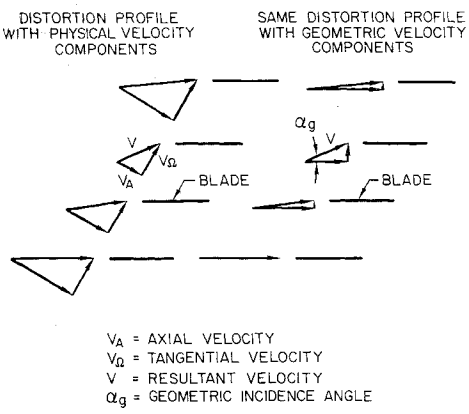

Fig. 1 Typical axial velocity distortion.

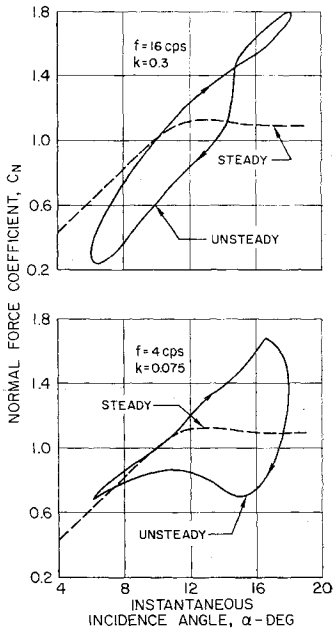

Fig. 2 Unsteady normal force loops for $\bar{\alpha}$ = 6°, M = 0.3, and α_M = 12°.

which is a plot of the stall-angle parameter σ as a function of circumferential position ϕ_D, where $\sigma = \alpha_g/\alpha_s$ and where α_g and α_s are the geometric and stalling incidence angles of the airfoil, respectively; both of these angles are measured relative to the zero lift condition. (In addition to the ϕ_D scale, a dimensionless scale, denoted by λ, has been provided which shows the fraction of the disturbance period.)

The shape of the hypothetical σ profile in Fig. 3 was chosen to have the following characteristics: 1) no sharp corners or sudden changes in curvature, 2) a region of relatively large rate of change, 3) a contrasting region of relatively little rate of change, 4) a significantly large change between the minimum and maximum values of σ, and 5) continuity at the end points. Additional versatility was obtained by providing a number of numerical scales for the abscissa, and by permitting the curve to be traversed in either the direction of increasing ϕ_D or decreasing ϕ_D.

Initial consideration will be given to the curve referred to the abscissa scale for which $0° \leq \phi_D \leq 360°$. This disturbance represents one excitation per revolution and is denoted by $E = 1$. For this case, a given rotor blade would be operating at $\sigma = 0.60$ at $\phi_D = 0°$ and would initially experience a sharp increase in incidence angle in the approximate range $90° < \phi_D < 130°$, with a penetration into stall (based on the geometric incidence angle) occurring at $\phi_D = 110°$. A peak value of $\sigma = 1.47$ at $\phi_D = 145°$ would be followed by a gentle decrease in σ over the range $160° < \phi_D < 310°$, after which the value of σ would return to its initial value of 0.60 at approximately $\phi_D = 340°$. This process would be repeated on each blade of the rotor, once per revolution. A change in abscissa scale to the range

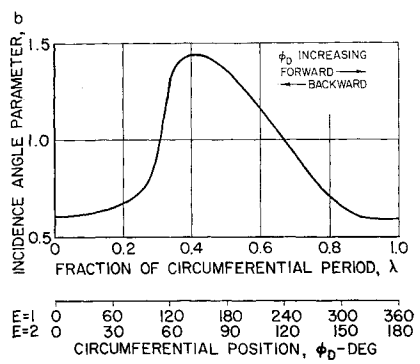

Fig. 3 Hypothetical distortion profile.

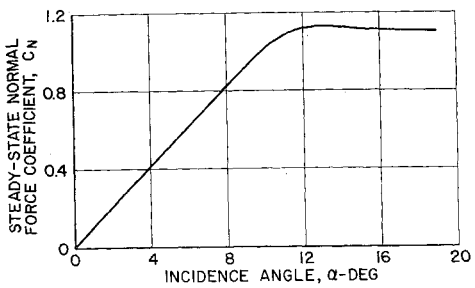

Fig. 4 Variation of steady-state normal force coefficient with incidence angle.

$0° \leq \phi_D \leq 180°$ (combined with a repetition of the same distortion over the range $180° \leq \phi_D \leq 360°$) would result in two excitations revolution. This is denoted by $E = 2$ in Fig. 3.

Finally, this profile may be traversed in two directions: a forward traverse, with ϕ_D increasing from left to right, and a backward traverse, with ϕ_D increasing from right to left (not shown in the abscissa scales to avoid confusion). Thus, a rotor immersed in a distortion having the forward profile will experience a sudden rise in geometric incidence, followed by a gentle decay back to some original value, and a rotor immersed in a distortion having the backward profile will experience a gentle increase in geometric incidence, followed by sudden decay back to its original value.

Steady-State Considerations

Before proceeding to the unsteady aspects of this problem, it is necessary to look briefly at both the steady-state characteristics of the original data and the quasi-steady aerodynamic response of a rotor blade operating in the distorted flow environment. The steady-state normal force variation with incidence angle obtained in the original study is plotted in Fig. 4. It is seen that the curve passes through the origin and has a zero slope at approximately $\alpha_s = 13°$, which will be defined as the stalling angle. Hence, the defining relationship for σ may be rewritten as $\alpha_g \cong 13\sigma$ (deg). This equation was used to convert the distortion profile from Fig. 3 into an equivalent circumferential geometric incidence angle distribution which, together with the steady-state curve in Fig. 4, yielded the result shown in Fig. 5. In this figure is found the circumferential quasi-steady normal force variation that would be imposed on a rotor blade by the given inlet distortion if the penetration into the distortion were to take place infinitely slowly. Both forward and backward traverses of the profile are represented here since the direction of penetration is almost meaningless in a quasi-steady response. The quasi-steady stall region is characterized by a shallow depression in the normal force curve as a function of λ.

Calculation Procedure

The distortion profile may now be converted into an equivalent variation of α_g, A, and B with ϕ. From the preceding, $\alpha_g \cong 13\sigma$, where α_g is in degrees. The angular velocity and acceleration are first rewritten as $\dot{\alpha} = (d\alpha/d\phi)\dot{\phi}$ and $\ddot{\alpha} = (d^2\alpha/d\phi^2)\dot{\phi}$, and the rotor speed is defined by $\Omega = \pi R/30 = \dot{\phi}$, where Ω is in rad/sec and R is rotor rpm. After these various relations are substituted into Eqs. (1) and (2), the result is

$$A = (\pi bR/30V)(d\alpha/d\phi) = (13\pi bR/30V)(d\sigma/d\phi_D) \quad (3)$$

$$B = (\pi bR/30V)^2(d^2\alpha/d\phi^2) = (13\pi bR/30V)^2(180/13\pi)(d^2\sigma/d\phi_D{}^2) \quad (4)$$

In these equations, α and ϕ are in radians, σ is dimensionless, and ϕ_D is in degrees. In practice, the σ distribution of the distortion profile will not necessarily be representable in a convenient form to permit direct differentiation in closed form. Hence, a numerical differentiation procedure employing central differences[1] was used in the present study.

Unsteady Aerodynamic Theory (Theodorsen)

A useful comparison may be made by employing Theodorsen's unsteady aerodynamic theory[2] to determine the unsteady normal force response of an unstalled airfoil operating over the same incidence range as the stalled airfoil but having a linear C_N, α characteristic. In view of the nonsinusoidal character of the incidence angle distribution, α was approximated by the general Fourier series

$$\alpha(\lambda) = \bar{\alpha}_0 + 2\sum_{n=1}^{\infty}[\bar{\alpha}_{nR}\cos 2\pi n\lambda - \bar{\alpha}_{nI}\sin 2\pi n\lambda] \quad (5)$$

and the unsteady normal force was computed from the formula

$$C_N(\lambda) = C_{N\alpha s}\left\{\bar{\alpha}_0 + \sum_{n=1}^{\infty}([U(nk)\bar{\alpha}_{nR} - W(nk)\bar{\alpha}_{nI}]\times \cos 2\pi n\lambda - [U(nk)\bar{\alpha}_{nI} + W(nk)\bar{\alpha}_{nR}]\sin 2\pi n\lambda)\right\} \quad (6)$$

In these equations the variable λ is the fraction of the circumferential period, and U and W are the unsteady aerodynamic functions. The details of the analysis are given in Appendix A.

Discussion of Results

The aerodynamic response curves are presented in Figs. 6–9. In each plot, the unsteady normal force variation obtained from the empirical data is represented by the solid line, that obtained from the Theodorsen theory by the dash-dot line, and the quasi-steady normal force by the dashed line. In addition to the dimensionless λ scale, a second scale has been used which indicates the physical extent of the disturbance period.

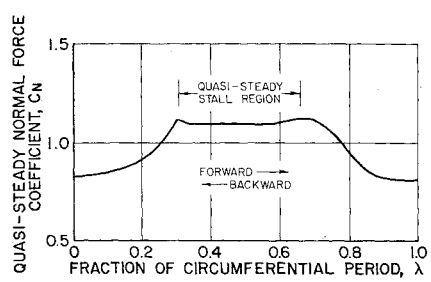

Fig. 5 Quasi-steady response to distortion profile.

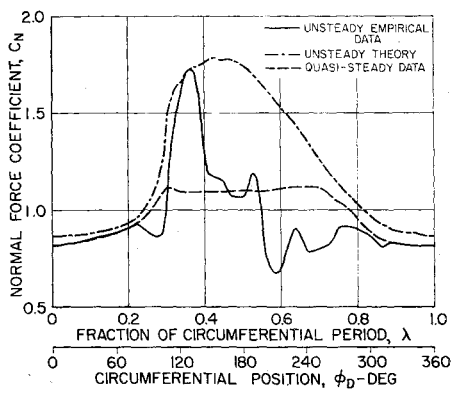

Fig. 6 Response to distortion profile for a forward traverse, $E = 1$.

The purpose of the present study is to investigate the unsteady stalling behavior of an airfoil or blade experiencing a dynamic change in incidence angle. To remain consistent in what is to follow, it is necessary to define what is meant by stall and what its characteristics must be in the case of an unsteady response. In general, an airfoil is said to stall when its lift or normal force no longer increases with increasing incidence angle. In many cases, the lift or normal force will actually decrease with increasing incidence angle beyond the stalling angle. This is clearly shown in Fig. 4, in which the stalling angle is defined to be $\alpha_s = 13°$, and it is seen that C_N decreases as α increases beyond 13°.

In the case of an unsteady motion, the definition of stall is not so clear-cut. Here the unsteady behavior must be evaluated relative to either the steady response or the unsteady theoretical response. An illustration of this statement is afforded by the two experimenta'ly determined normal force loops shown in Fig. 2, for frequencies of 4 and 16 cps, and their comparison with the superimposed steady-state normal force variation. It is seen that in both cases the unsteady lift attains a value far in excess of the steady-state value during the portion of the motion for which incidence increases. However, the normal force response is quite different for the two frequencies when the incidence angle decreases. At low frequency the normal force drops off sharply and remains at a value considerably below the steady-state value over a large incidence range. In contrast to this, at high frequency the unsteady normal force returns to its starting value by a nearly elliptical path, and its value is only slightly lower than the steady-state value at each incidence angle along the return path.

The unsteady normal force variation on an actual compressor blade in a distortion environment will probably follow that predicted by the unsteady empirical data. The unsteady stalling characteristics of such a blade when plotted as a function of λ can be evaluated either by noting the value of λ at which the unsteady empirical normal force curve penetrates below the quasi-steady normal force curve and the range of λ over which it remains significantly below the quasi-steady curve, or by investigating the way in which the unsteady empirical normal force curve departs from the theoretical curve. Both of these methods were employed in the present study, and both were found to be in very good qualitative agreement and in fair quantitative agreement.

Consider first Figs. 6 and 7 for a forward traverse of the distortion profile for $E = 1$ and 2, respectively. In both cases, the unsteady empirical normal force response (solid line) initially dips below the steady-state curve (dashed line), then rises sharply to a maximum value of C_N in excess of 1.7, which is considerably greater than the maximum possible steady-state value. This is followed by a decrease in unsteady empirical C_N to a value smaller than the steady-state value, after which the unsteady value eventually returns to approximately the quasi-steady level. In both

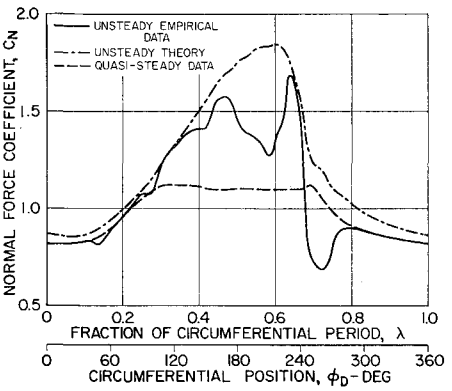

Fig. 8 Response to distortion profile for a backward traverse, $E = 1$.

figures the unsteady normal force curves obtained from potential flow theory are very similar to one another. Since these curves are based on linear theory in which stalling does not occur, they generally follow the σ variation, and any departures of the theoretical curves from the σ profile shape occur as a result of unsteady hysteresis effects. [The theoretical curves were calculated using the first twenty harmonics of the Fourier series in Eq. (6).]

In Fig. 6, for $E = 1$, the empirical response initially increases as the theoretical response increases, but breaks away sharply from the theoretical curve at approximately $\lambda \cong 0.35$, decreases rapidly, and penetrates below the quasi-steady curve at approximately $\lambda \cong 0.45$. The empirical curve does not return to the level of either the theoretical or the quasi-steady curve until $\lambda \cong 0.8$. Thus, relative to the quasi-steady response, dynamic stall occurs over 35% of the period ($0.45 \leq \lambda \leq 0.8$), and relative to the theoretical response, it occurs over 45% of the period ($0.35 \leq \lambda \leq 0.8$).

Similarly, in Fig. 7, for $E = 2$, the dynamic stall persists over approximately the same range of λ as for $E = 1$, according to both criteria just used. Note, however, that in going from $1E$ to $2E$ (Fig. 6 to Fig. 7), that region in which the unsteady empirical normal force is substantially greater than the quasi-steady normal force is considerably enlarged. Note also that the choice of the recovery point is somewhat arbitrary since this is a region of relatively low normal force, and with an oscillating empirical curve it is difficult to choose between a point at 0.8 and at 0.95. Thus, although the stalled percentage of the period for $E = 2$ is approximately the same as that for $E = 1$, a general observation of the two response curves indicates that the higher-order disturbance may not be as detrimental in the generation of stall as the first-order disturbance. This trend was observed in calculations carried out for a number of additional cases.[3] The quantitative results indicated that as the number of dis-

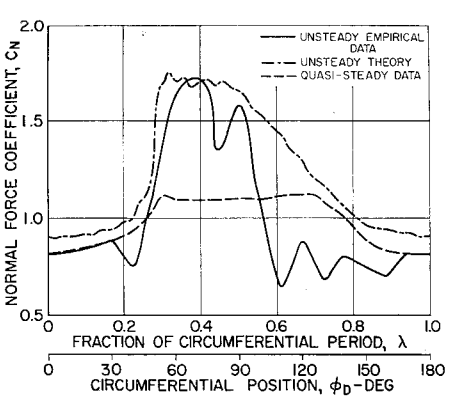

Fig. 7 Response to distortion profile for a forward traverse, $E = 2$.

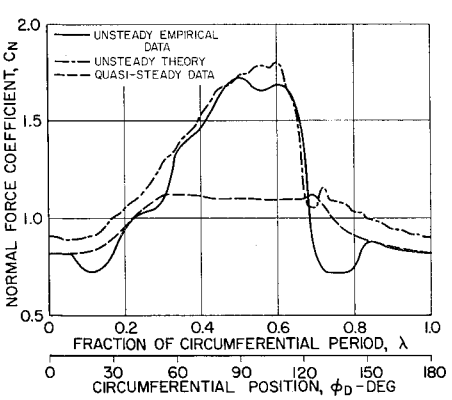

Fig. 9 Response to distortion profile for a backward traverse, $E = 2$.

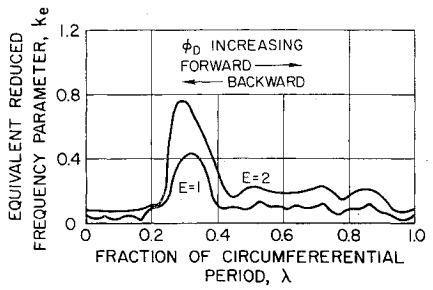

Fig. 10 Variation of k_e with circumference.

turbances per revolution increases, the region of stall-like response either remains approximately the same or becomes smaller for all cases considered to date.

Of even greater importance are the results indicated in Figs. 8 and 9, in which the backward traverse of the distortion profile has been employed. For example, in Fig. 8 for $E = 1$, it is seen that the empirical response, although somewhat irregular, doesn't break away completely from the theoretical response until $\lambda \cong 0.65$, which is approximately the same value at which the empirical curve penetrates the quasi-steady curve. Recovery, according to both criteria, occurs for $\lambda < 0.8$, and thus the stalled condition extends over less than 15% of the period. For $E = 2$, shown in Fig. 9, the same penetration and recovery conditions prevail, and once again stall occurs over less than 15% of the period. In this case, however, the increased effective frequency of the disturbance has caused a considerable smoothing of the response relative to that of the first-order disturbance. In fact, the empirical response is very nearly the same as the theoretical response over much of the period.

Thus, it is seen from these figures that for the particular profile chosen for this study, a forward traverse is more detrimental to the blade stalling characteristics than the backward traverse. In terms of the size of the stalled portion of the period, a forward traverse produces stall over approximately 30 to 45% of the period, whereas a backward traverse of the same profile produces stall over 10–15% of the period. In an effort to understand these differences between the forward and backward traverses, the following heuristic approach was used. The local rate of change of σ was related to an "equivalent" reduced frequency k_e; the details of the construction of k_e will be found in Appendix B. In effect, k_e is the reduced frequency at each value of λ for an "equivalent" sinusoidal motion which satisfies the local values of A and B.

Now consider the distortion profile in detail. It is seen in Fig. 3 that a forward traverse involves a rapid increase followed by a gradual decrease in incidence angle, and a backward traverse involves a gradual increase followed by a rapid decrease in incidence angle. The angular velocity parameter will be large during the rapid change portion of the σ profile, and small during the gradual change portion of the σ profile. From the positive definite form of Eq. (B1) (see Appendix B), it is seen that k_e will also be large over the region of rapid change in σ and small over the region of gradual change. This is shown in Fig. 10, in which the variation of k_e with λ is plotted for $E = 1$ and 2. The direction of forward and backward traverses is indicated by arrows.

The curves in Figs. 2, 3, and 10 will serve to explain why the forward and backward traverses of the given profile for a given order disturbance yield such large differences in the stalling behavior of a blade subjected to this flow environment. From Fig. 2 it can be seen that for both low and high values of the frequency, a continual increase in incidence angle produces a continual increase in unsteady normal force, up to some peak value of C_N, which occurs at or near the peak value of α. However, a marked difference in aerodynamic response is evident for the decreasing incidence-angle regime; viz., at high frequency the normal force continues to respond as though the flow were unstalled (with the exception of a few minor differences), but at low frequency the normal force decreases suddenly and exhibits all the characteristics of a stalled flow. Thus, for sinusoidal motion, whether k is large or small, there will be little apparent effect on the response of C_N during an increase in α to a value above the stalling incidence. Except for very small values of k, the unsteady normal force will generally increase to a value greater than the maximum steady-state C_N. However, during a decrease in α from a value above the stalling incidence, the normal force response will be profoundly affected by the value of k; if k is large, a generally unstalled C_N response will be observed, whereas if k is small, a stalled condition will prevail.

A comparison between Figs. 3 and 10 shows that k_e will be large over the steep portion of the σ curve (between $0.2 < \lambda < 0.4$) and will be small over the remainder of the σ curve. If the σ profile is traversed in the forward direction (i.e., from left to right), the largest values of k_e occur during the rise is incidence angle, and smaller values of k_e occur during the decrease in incidence angle. Thus, according to the evidence in Fig. 2, the lower effective frequency for decreasing incidence angle leads to a large dynamic stall. Conversely, if the backward profile is traversed (i.e., from right to left), the largest values of k_e occur during the decrease in incidence angle. In this case, the higher effective frequency for decreasing incidence angle suppresses the tendency for dynamic stall to occur.

Concluding Remarks

For the particular distortion profile under consideration, it was found that

1) For increasing incidence angle, the rate of change of incidence angle had relatively little effect on the unsteady normal force response, the maximum value of which generally exceeded the steady-state normal force response by a considerable margin.

2) For decreasing incidence angle, it was possible to encounter a severe stalling of the blade. The severity was dependent on the factors enumerated below.

3) With decreasing incidence angle, a large rate of change of incidence produced a smaller region of dynamic stall than did a small rate of change of incidence; this appeared to be a very strong dependency and yielded a greater change in dynamic stall behavior than did the other parametric variations.

4) An increase in the order of the disturbance (from 1 to 2 disturbances per revolution) tended to reduce the region of severe dynamic stall.

Appendix A: Derivation of Formulas for Fourier Analysis

From p. 280 of Ref. 4, the unsteady normal force on an airfoil executing a single-degree-of-freedom sinusoidal pitching oscillation about a pivot axis at a, relative to the midchord, and having a zero mean incidence angle, is given by

$$N = -\pi\rho b^3\omega^2[L_\alpha - (\tfrac{1}{2} + a)L_h]\bar{\alpha}e^{i\omega t} \qquad \text{(A1)}$$

where L_h and L_α are complex functions defined in Ref. 5 as

$$k^2L_h = k^2 + 2kG - 2ikF \qquad \text{(A2)}$$

$$k^2L_\alpha = \tfrac{1}{2}k^2 + 2kG - 2F - i(k + 2kF + 2G) \qquad \text{(A3)}$$

and where $\bar{\alpha}e^{i\omega t}$ is a complex representation of the instantaneous incidence angle measured relative to the reference mean angle which for now is taken to be zero. F and G are the real and imaginary parts, respectively, of the Theodorsen function $C(k) = F(k) + iG(k)$. The unsteady normal force coefficient for a pitching oscillation about a zero mean incidence angle will be obtained by dividing Eq. (A1) by the

product $\rho V^2 b$, and after using Eqs. (A2) and (A3), the result is given by

$$C_N = \pi(U + iW)\bar{\alpha}e^{i\omega t} \tag{A4}$$

where, for convenience, U and W have been defined as

$$U(k) = ak^2 + 2F - 2(\tfrac{1}{2} - a)kG \tag{A5}$$

$$W(k) = k + 2G + 2(\tfrac{1}{2} - a)kF \tag{A6}$$

If the reduced frequency k is set equal to zero, Eq. (A4) yields the steady-state normal force coefficient $C_N(k = 0) = 2\pi\bar{\alpha}$ where 2π is the theoretical slope of the normal force curve. Hence, in order that Eq. (A4) represent a more general class of normal force functions, the factor 2π will be replaced by the actual slope of the normal force curve, or, $\pi \rightarrow C_{N\alpha_s}/2$, and Eq. (A4) will become

$$C_N = \tfrac{1}{2}C_{N\alpha_s}(U + iW)\bar{\alpha}e^{i\omega t} \tag{A7}$$

where $C_{N\alpha_s} = (\partial C_N/\partial\alpha)_{\text{steady state}}$. In Fig. 4 the linear range of the steady-state curve has a slope of 0.520/5 $(\text{deg})^{-1}$ or, equivalently, $C_{N\alpha_s} = 5.96/\text{rad}$.

Equation (A7) represents the normal force response to a harmonic motion of frequency ω. By superposition, the response to any arbitrary periodic motion may be obtained through the use of the concept of complex admittance.[4] For convenience, the substitution $\omega t = 2\pi\lambda$ will be made, where $\lambda = t/T$ is the fraction of the period and varies over the range $0 \leq \lambda \leq 1$. Then the general motion will be given by

$$\alpha(\lambda) = \sum_{n=-\infty}^{\infty} \bar{\alpha}_n e^{in\omega t} = \sum_{n=-\infty}^{\infty} \bar{\alpha}_n e^{2i\pi n\lambda} \tag{A8}$$

and the general response is

$$C_N(\lambda) = \frac{1}{2} C_{N\alpha_s} \sum_{n=-\infty}^{\infty} [U(nk) + iW(nk)]\bar{\alpha}_n e^{2i\pi n\lambda} \tag{A9}$$

The fundamental disturbance will have a period $T = 60/RE$ (sec/excitation) where R is rotor rpm and E is the number of excitations/revolution. Hence, the fundamental frequency is $\omega = 2\pi/T = \pi RE/30$, and the fundamental reduced frequency is $k = \pi REb/30V$.

The only remaining unknowns in Eqs. (A8) and (A9) are the Fourier coefficients $\bar{\alpha}_n$. These can be obtained from the given distribution of $\alpha(\lambda) = 13\pi\sigma(\lambda)/180$ by application of the orthogonality conditions on Eq. (A8). The result is

$$\bar{\alpha}_n = \int_0^1 \alpha(\lambda)e^{-2i\pi n\lambda}\, d\lambda \tag{A10}$$

In their present form, Eqs. (A8) and (A9) require summation over negative values of n and hence are inconvenient to use for calculating the final response functions. This difficulty is easily eliminated, as shown below. In Eq. (A10), $\alpha(\lambda)$ is a pure real function, and hence

$$\bar{\alpha}_n = \bar{\alpha}_{nR} + i\bar{\alpha}_{nI} \tag{A11}$$

is complex. Furthermore, $\bar{\alpha}_{nR}$ is even and $\bar{\alpha}_{nI}$ is odd, relative to the index n; hence

$$\bar{\alpha}_{-n} = \bar{\alpha}_{-nR} + i\bar{\alpha}_{-nI} = \bar{\alpha}_{nR} - i\bar{\alpha}_{nI} \tag{A12}$$

It can be shown that $F(nk)$ and $G(nk)$ are even and odd functions, respectively, relative to the index n. Hence it can be shown that $U(nk)$ is even, and $W(nk)$ is odd. When these quantities are substituted into Eqs. (A8) and (A9), the summation over negative n may be eliminated. The final results are presented in Eqs. (5) and (6). In these equations, $\bar{\alpha}_0$ is the average value of the $\alpha(\lambda)$ distribution. It is obtained from Eq. (A10) for $n = 0$:

$$\bar{\alpha}_0 = \int_0^1 \alpha(\lambda)d\lambda \tag{A13}$$

Similarly, the Fourier coefficients $\bar{\alpha}_{nR}$ and $\bar{\alpha}_{nI}$ are given by

$$\bar{\alpha}_{nR} = \int_0^1 \alpha(\lambda)\, \cos 2\pi n\lambda d\lambda \tag{A14}$$

$$\bar{\alpha}_{nI} = -\int_0^1 \alpha(\lambda)\, \sin 2\pi n\lambda d\lambda \tag{A15}$$

Appendix B: Equivalent Reduced Frequency

The equivalent reduced frequency is obtained by assuming that the σ distribution can be approximated at each point by a sinusoid that satisfies the local values of A and B according to the relationships in Eqs. (1) and (2). In these equations, A and B may be regarded as known quantities, computed from the σ distribution using Eqs. (3) and (4), and α may also be obtained from σ by the formula $\alpha = 13\pi\sigma/180$. If it is assumed that $\bar{\alpha} = (\alpha_{\max} - \alpha_{\min})/2$, then the only unknown quantities in Eqs. (1) and (2) are the equivalent values of k and α_M. A simultaneous solution of these equations yields the useful approximation for k_e,

$$k_e = \{[A^2 + (A^4 + 4\bar{\alpha}^2B^2)^{1/2}]/2\bar{\alpha}^2\}^{1/2} \tag{B1}$$

References

[1] Milne-Thomson, L. M., *The Calculus of Finite Differences* (MacMillan and Company Ltd., London, 1933).

[2] Theodorsen, T., "General theory of aerodynamic instability and the mechanism of flutter," NACA Rept. 496 (1935).

[3] Carta, F. O., "The unsteady normal force response of an airfoil in a periodically distorted inlet flow including stalling effects," United Aircraft Corp. Research Labs. Rept. E211116-1 (January 1966).

[4] Bisplinghoff, R. L., Ashley, H., and Halfman, R. L., *Aeroelasticity* (Addison-Wesley Publishing Company Inc., Reading, Mass., 1955).

[5] Scanlan, R. H. and Rosenbaum, R., *Introduction to the Study of Aircraft Vibration and Flutter* (The MacMillan Co., New York, 1951).